JOURNAL OF CATALYSIS **177,** 224–230 (1998)
ARTICLE NO. CA982097

Selective Oxidation of *n*-Butane to Maleic Anhydride on Vanadyl Pyrophosphate

II. Characterization of the Oxygen-Treated Catalyst by Electrical Conductivity, Raman, XPS, and NMR Spectroscopic Techniques

K. Aït-Lachgar,* A. Tuel,* M. Brun,* J. M. Herrmann,† J. M. Krafft,‡ J. R. Martin,‡ J. C. Volta,* and M. Abon*,[1]

*Institut de Recherches sur la Catalyse, CNRS, 2 Avenue Albert Einstein, 69626 Villeurbanne, Cedex, France; †URA au CNRS, Photocatalyse, Catalyse et Environnement, Ecole Centrale de Lyon, BP 163, 69131 Ecully, Cedex, France; and ‡Laboratoire de Physico-Chimie des Interfaces, Ecole Centrale de Lyon, BP 163, 69131 Ecully, Cedex, France

Received December 2, 1997; revised March 26, 1998; accepted March 26, 1998

In a previous publication (*J. Catal.* 171, 383 (1997)) we have shown that the oxidation of a pure and well-crystallized $(VO)_2P_2O_7$ catalyst at 500°C for different times improves the catalytic performance in the *n*-butane selective oxidation to maleic anhydride. This has been explained by a proper density of selective V^V species associated with structural defects. In the present work we bring additional information on the nature of the $V^{(V)}$ species formed during oxidation. By using electrical conductivity, Raman, XPS, and ^{31}P NMR (spin echo mapping and MAS), it is concluded that: (i) Upon oxygen exposure, isolated V^V species appear at the surface but also in the bulk of $(VO)_2P_2O_7$ (V^{IV} phase) within some depth without the formation of any definite $VOPO_4$ (V^V phase) phase. (ii) A suitable $V^{(V)}/V^{(IV)}$ ratio around 0.25 is suggested by XPS analysis for the best catalytic performance. For longer oxidation treatments, the development of amorphous $V^{(V)}$ microdomains occurs. The formation of such domains is detrimental to *n*-butane selective oxidation.

Key Words: ***n*-butane partial oxidation; maleic anhydride; oxidized vanadyl pyrophosphate; $V^{(V)}$ species; electrical conductivity; XPS; LRS; NMR.**

INTRODUCTION

In the first part of the present work (1), we have investigated the effect of oxidizing treatments (at 500°C) on the catalytic performances in *n*-butane oxidation of a pure and well-crystallized $(VO)_2P_2O_7$ phase. This relatively low temperature of oxidation was chosen in order to avoid (or limit) the bulk oxidation of $(VO)_2P_2O_7$ to $VOPO_4$ phases which would be poorly active and/or selective (2–4). For a time of oxidation of 1 h, we observed that the selectivity to maleic anhydride strongly increased from 52 to 84%, whereas the activity remained virtually the same.

The prevalent effect of V^{5+} on the selectivity is in line with a redox mechanism previously investigated by ^{18}O-labelling (5) and electrical conductivity (6). V^{5+} species would be most likely involved in the oxygen insertion steps, especially the last step from furan to maleic anhydride (MA) (7, 8). XRD spectra previously reported in the first part of the present work (1) did not allow us to detect the formation of any definite $VOPO_4$ phase but indicated the creation of structural disorder induced by the oxygen exposure. Clearly, more work was needed to better characterize the changes in the catalysts induced by the oxygen treatment. For this purpose we used electrical conductivity, laser Raman spectroscopy, ^{31}P NMR (spin-echo mapping and MAS), and surface analysis by XPS.

EXPERIMENTAL

The preparation of the reference $(VO)_2P_2O_7$ catalyst (PYRO) and of the oxidized $(VO)_2P_2O_7$ catalysts (PYRO-OX) has been described in the first part of the present work (1) mainly devoted to the catalytic performance of the catalysts. The fresh and the oxidized catalysts have been already characterized by XRD, TGA-DTA, and UV-VIS spectroscopy (1).

In-Situ Electrical Conductivity Measurements

We used a cell specially designed to measure the electrical conductivity of powdered samples (9). The electrical conductivity of the pyrophosphate samples was measured at 400°C under oxygen (16.7 kPa), *n*-butane (1.47 kPa), and the reaction mixture with a ratio (O_2/*n*-C_4H_{10} : 125/11) as in

[1] To whom correspondence should be addressed.

0021-9517/98 $25.00

catalytic tests. Similar experimental conditions have been used in our previous studies on V-P-O catalysts (6, 10).

Raman Spectroscopy

Raman spectra in the 800–1200 cm^{-1} range were recorded by means of a DILOR OMARS 89 spectrometer equipped with an intensified multichannel photo-diode array detector. The laser beam (514.5 nm) was scanned on the sample surface by means of a rotating lens in order to limit thermal effect and/or photodegradation. Further experimental details can be found in previous studies (11, 12).

^{31}P NMR Analysis

^{31}P NMR spectra were acquired on a Bruker DSX 400 spectrometer operating at 161.9 MHz using a 4-mm standard probe head. Details concerning the acquisition of ^{31}P spin echo mapping (^{31}P NMR SEM) spectra have been reported earlier (13). ^{31}P MAS spectra were obtained at a spinning speed of 12 KHz with a pulse length of 1.5 μs ($\pi/4$) and a recycle delay of 60 s.

XPS Analysis

XPS analysis was performed in a VG ESCALAB 200R machine using the MgKα radiation. The electric charge was corrected by setting the binding energy (BE) of adventitious carbon (C_{1s}) at 284.5 eV. For quantitative analysis, we used the integrated area under $V_{2p3/2}$, O_{1s}, P_{2p}, and C_{1s} peaks after smoothing and subtraction of a nonlinear Shirley background.

For quantitative analysis we used the sensitivity factors provided by the VG software and the differences in mean free path of the photoelectrons have been considered. The relative percentage of surface V^V and V^{IV} species has been estimated ($\pm 10\%$) from the $V_{2p3/2}$ peak using a peak decomposition and curve-fitting technique (14, 15).

RESULTS

Electrical Conductivity Measurements

The changes in electrical conductivity (σ) induced by the sequential introduction of the reactants (*n*-butane and then oxygen) and the reaction mixture (n-$C_4H_{10} + O_2$) have been compared at 400°C (the usual reaction temperature) for the $(VO)_2P_2O_7$ catalyst (denoted PYRO) and for the same sample previously treated *in-situ* under oxygen (16.7 kPa) for 1 h at 500°C (PYRO-OX-1), as shown in Fig. 1.

Note first that the initial steady state of the conductivity for the oxidized sample is almost 10 times higher than for the PYRO sample. After a prompt evacuation of oxygen, the introduction of C_4H_{10} (1.47 kPa) induced a sharp decrease of σ for both samples. For the oxidized catalyst, the kinetics of reduction by butane was less rapid than for the PYRO sample, most likely as a result of an excess of oxygen associated with V^{5+} surface species. For the PYRO sample, there was an instantaneous σ decrease, followed by a slow increase towards a final steady state value. Such behavior suggests that the initial reduction by butane is followed by a slow reoxidation of the surface region, most likely by slow oxygen anion diffusion from the sublayers. This behavior is quite reproducible when compared to previous results (6).

The subsequent evacuation of butane and its replacement by O_2 induced an immediate increase of σ for both samples. This increase was even more important for the oxidized sample ($\Delta \log \sigma > 4$), which recovered exactly its initial conductivity.

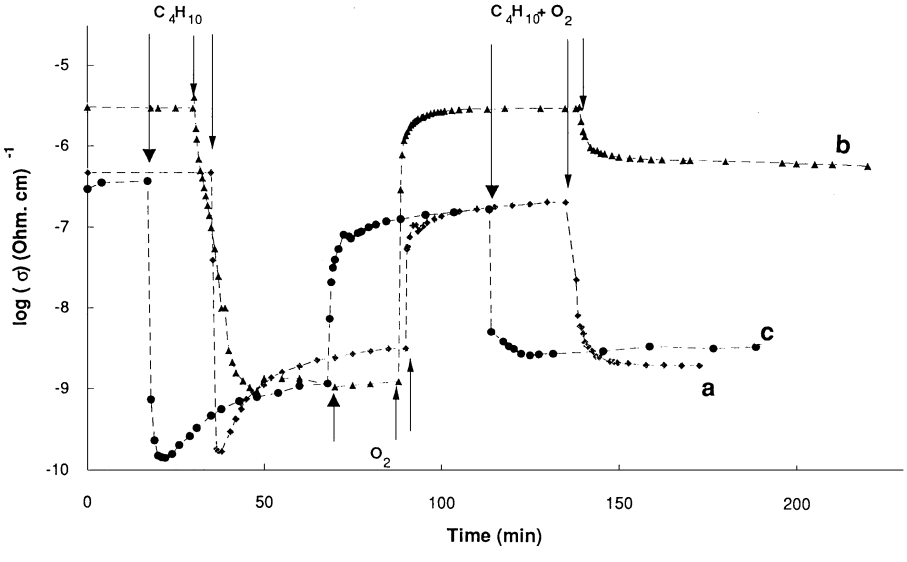

FIG. 1. Variation of the electrical conductivity of PYRO (a), PYRO-OX-1 (b), and PYRO-OX-3 after hot water leaching (c) at 400°C under sequential exposures to *n*-butane, oxygen, and reaction mixture.

After subsequent introduction of the reaction mixture, σ decreased as expected by the presence of *n*-butane but the decrease was more limited for the oxidized sample. σ changes were therefore qualitatively similar for both samples. σ strongly decreased upon reduction by butane and sharply increased upon oxidation by oxygen. Such behavior is characteristic of a *p*-type semiconductor as previously discussed (6). In contrast to $(VO)_2P_2O_7$, $VOPO_4$ phases were previously characterized as extrinsic *n*-type semiconductors (10). However, σ changes appeared more strongly marked on the oxidized sample with a large difference (by more than four orders of magnitude) of conductivity between the reduced and the oxidized state. Moreover, it is noteworthy to remark that the conductivity level under the reaction mixture for the oxidized sample is about 500 times higher than for the same sample before any oxidation.

It is known that V^{5+} can be substantially removed by hot water leaching (1, 3). After such a treatment in boiling water the sample oxidized for 3 h has an electrical behavior identical to the initial untreated catalyst (Fig. 1). This indicates that V^{5+} ions were mainly concentrated at the surface or within the first sublayers of the solid, in agreement with previous results (1) and with those obtained further in the present article with other techniques (Raman, XPS, and ^{31}P NMR).

Raman Spectroscopy

The influence of the oxygen treatments at 500°C on the Raman spectrum of $(VO)_2P_2O_7$ is summarized in Fig. 2. The initial spectrum (Fig. 2a) is characteristic of a pure and well-crystallized $(VO)_2P_2O_7$ phase with characteristic bands at 923, 933, 1135, and 1189 cm^{-1} (11). With increasing time of oxygen treatments up to 24 h, the spectra (2b, 2c, 2d) mainly show the progressive development of an additional band at about 1038 cm^{-1}.

After hot water leaching, the sample oxidized for 24 h displays a spectrum (Fig. 2e) virtually identical to the spectrum of the starting $(VO)_2P_2O_7$ catalyst (Fig. 2a). This observation also shows that V^{5+} species were mainly located within a few surface layers in agreement with previous results (1).

The comparison with the Raman spectra of the various $VOPO_4$ phases, previously studied by Ben Abdelouhab *et al.* (11), suggests that the new band at 1038 cm^{-1} could be attributed to α_I-$VOPO_4$. Therefore we have prepared for comparison the α_I-$VOPO_4$ phase by calcination in air of the dihydrate, $VOPO_4$, $2H_2O$, at 650°C for 6 h (11). Its Raman spectrum (Fig. 2f) is in agreement with previously obtained spectra (3, 11). The band at 1038 cm^{-1} has been attributed to a V-O-P coupled stretching vibration (3, 11). There is some similarity between the spectrum of α_I-$VOPO_4$ (Fig. 2f) and the spectrum of the oxidized pyrophosphate (Fig. 2d), although the band at 1038 cm^{-1} is actually less developed, in agreement with a sample not too deeply oxidized where the main phase is still $(VO)_2P_2O_7$.

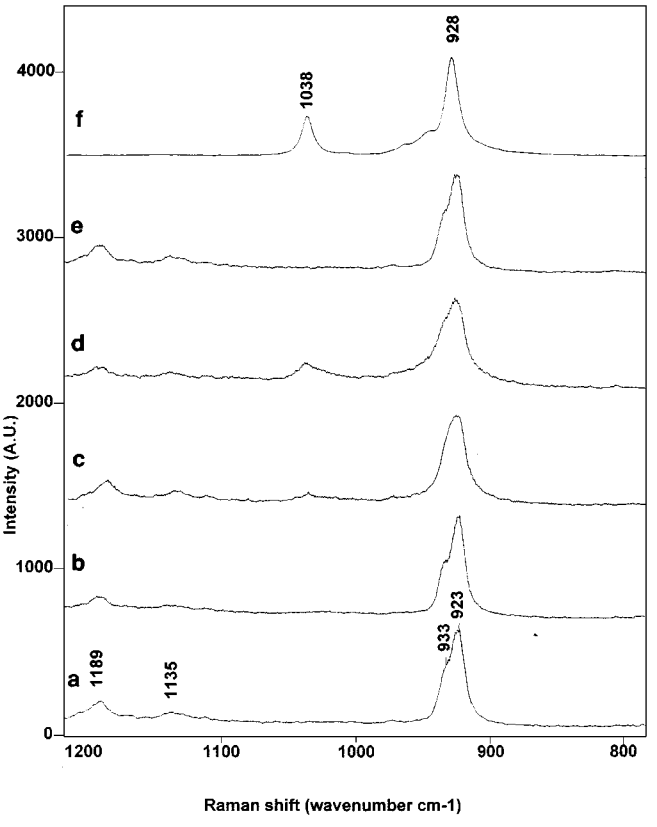

FIG. 2. Laser Raman spectra of PYRO (a), PYRO-OX-1 (b), PYRO-OX-12 (c), PYRO-OX-24 (d), and PYRO-OX-24 after hot water leaching (e), and α_I-$VOPO_4$ (f).

It is already known that all $VOPO_4$ phases (with the exception of β-$VOPO_4$) are very sensitive to hydration, especially α_I-$VOPO_4$ which is rapidly converted to $VOPO_4$, $2H_2O$ upon exposure to air moisture (3, 12). Such rapid changes did not occur for the oxidized sample, (PYRO-OX-24), the Raman spectrum of which (Fig. 2d) was not much altered after air exposure for 10 days, with no evidence of any formation of $VOPO_4$, $2H_2O$. Therefore there is some doubt on the actual presence of α_I-$VOPO_4$ in the oxidized pyrophosphate samples.

XPS Analysis

Comparative XPS analysis was performed on the starting pyrophosphate catalyst and on the same sample oxidized for 1 and 3 h at 500°C. The sample oxidized for 3 h and afterwards submitted to hot water leaching was also examined. The analysis on these samples (atomic ratios) is summarized in Table 1. As discussed in previous XPS studies (5, 14, 16), the P/V and O/V ratios exceeded the stoichiometric value. The oxidation treatments and the subsequent water leaching did not change significantly the P/V and O/P ratios. This could mean that the surface structure and composition are actually different from the bulk one in

TABLE 1

Atomic Ratios Measured by XPS on the Studied Catalysts

Sample	P/V	O/V	O/P	C/V
PYRO	1.83	6.32	3.44	0.94
PYRO-OX-1	1.89	6.49	3.44	0.56
PYRO-OX-3	1.96	6.86	3.51	0.65
PYRO-OX-3 after H_2O leaching	1.79	6.46	3.62	0.65

$(VO)_2P_2O_7$ as discussed in a recent work using low energy ion scattering, in addition to XPS (16).

XPS was mainly used in an attempt to follow the extent of oxidation of surface vanadium, induced by the oxygen treatment at 500°C. As shown in Table 2, the binding energy (BE) of the $V_{2p3/2}$ peak was shifted from 517.1 eV (pyrophosphate sample) to 517.5 eV on the sample oxidized for 3 h, in agreement with the development of V^{5+} surface species. Table 2 also shows the relative percentage of V^{4+} and V^{5+} as estimated from a decomposition of the $V_{2p3/2}$ peak as previously described (14). For 3 h of oxidation, the relative V^{5+} surface percentage increased from 15 to 42%; it is worth noting that V^{4+} ions were still prevalent. XPS analysis also confirmed that hot water leaching was quite efficient in removing V^{5+} species; the sample was afterwards virtually identical to the starting pyrophosphate catalyst with respect to XPS analysis (Table 2).

NMR Spectroscopy

^{31}P NMR SEM spectra of the various catalysts show a main peak at ca 2600 ppm characteristic of $(VO)_2P_2O_7$ along with a signal near 0 ppm which increases with the time of oxygen treatment at 500°C (Fig. 3). The latter signal, which is not observed on the starting material, is typical of phosphorus atoms bonded to diamagnetic V^{5+} centers (13, 14). The V^{5+}/V^{4+} ratio, estimated by measuring the area of the signals at ca 0 and 2600 ppm, respectively, rises to 0.155 for PYRO-OX-24 but decreases to 0.065 (as indicated in Fig. 3) upon washing the sample with hot water, indicating that some of the V^{5+} species have been removed. A close

TABLE 2

XPS Binding Energy (BE) of the $V_{2p3/2}$ Level and Percentage of V^{4+} and V^{5+} on the Studied Catalysts

Sample	BE ($V_{2p3/2}$) (eV)	V^{4+} (%)	V^{5+} (%)
PYRO	517.1	85	15
PYRO-OX-1	517.2	80	20
PYRO-OX-3	517.5	58	42
PYRO-OX-3 after H_2O leaching	517.1	85	15

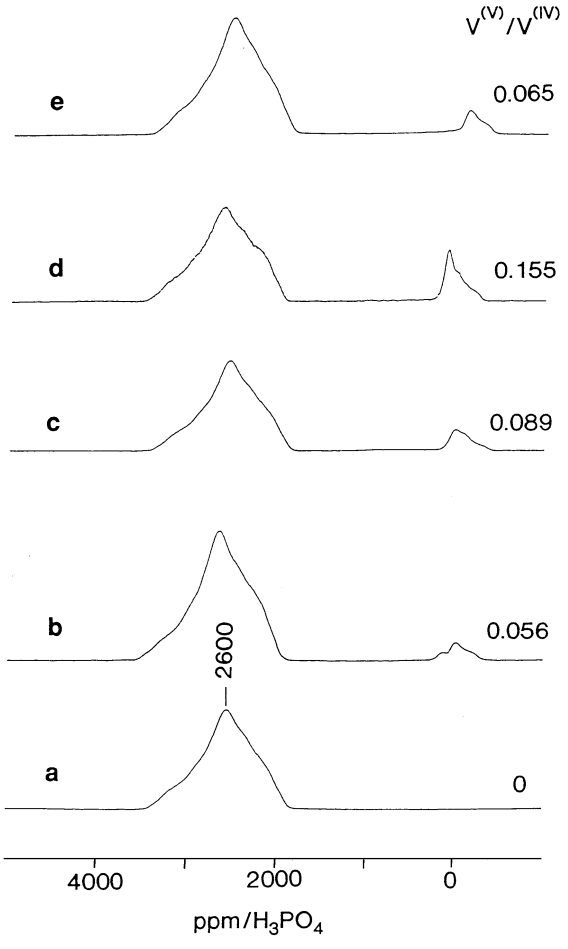

FIG. 3. ^{31}P NMR spin-echo mapping spectra of PYRO (a), PYRO-OX-1 (b), PYRO-OX-3 (c), PYRO-OX-24 (d), and PYRO-OX-24 after hot water leaching (e).

examination of the NMR signal around 0 ppm shows that it is actually composed of two components that differ not only by their position but also by their chemical shift anisotropy (CSA). The first one, with a relatively small CSA and a maximum intensity at ca 90 ppm is poorly developed on PYRO-OX-1 but increases with the oxidation time (Fig. 4). Its relative contribution to the NMR signal between +300 and −500 ppm increases from 18% for PYRO-OX-1 to 53% for PYRO-OX-24 as indicated in Fig. 4. The second component is characterized by an axially symmetric chemical shift tensor with $\sigma_\perp \approx -25$ ppm and $\sigma_{||} \approx -300$ ppm. Washing PYRO-OX-24 with hot water results in the complete disappearance of the first signal at 90 ppm, whereas the second component is not affected. ^{31}P NMR MAS spectra of the corresponding oxidized catalysts are composed of a major signal at −13.6 ppm along with a broad spinning sideband pattern and minor peaks at 3.5 and 7.6 ppm in Fig. 5.

Experiments performed at various spinning speeds showed that the isotropic chemical shift of the broad signal was −177.6 ppm. The comparison of the MAS spectra in

Fig. 5 with SEM spectra in Fig. 4 indicates that peaks at −13.6 and −177.6 ppm (Fig. 5) correspond to the isotropic chemical shifts associated with the two signals at 90 and −25 ppm (Fig. 4), respectively. The main signal at −13.6 ppm observed in the MAS spectra of the oxidized catalysts cannot be attributed to any crystalline $VOPO_4$ phase (3, 11, 13, 14). In particular, the chemical shift is very different from that of α_I-$VOPO_4$ ($\delta = 3.6$ ppm/H_3PO_4), whose presence in the catalysts was surmised on the basis of Raman spectroscopy data (Fig. 2).

Nevertheless, the minor peak at 7.6 ppm could be attributed to traces of the dihydrate phase $VOPO_4, 2H_2O$ ($\delta =$ 7.7 ppm/H_3PO_4), resulting from the hydration of $VOPO_4$ phases (3, 12). Actually, the identification of the V^{5+} phases present in oxidized catalysts is difficult due to their amorphous character as evidenced by XRD (1). This feature probably significantly increases their NMR line widths. Therefore, it is possible that such a chemical shift (−13.6 ppm) results from a mixture of amorphous precursors of α_{II}-, δ-, and β-$VOPO_4$ phases, commonly observed in VPO catalysts (14) and whose ^{31}P chemical shifts are located between −10 and −20 ppm. Moreover, these phases are known to be soluble in hot water and their presence would explain the disappearance of the signal upon washing the oxidized catalysts.

The interpretation of the second signal with an isotropic chemical shift at ca −177.5 ppm is more puzzling. Similar static line shapes have already been reported by Nguyen *et al.* (17) on spectra of pyrophosphate catalysts containing various amounts of structural defects. According

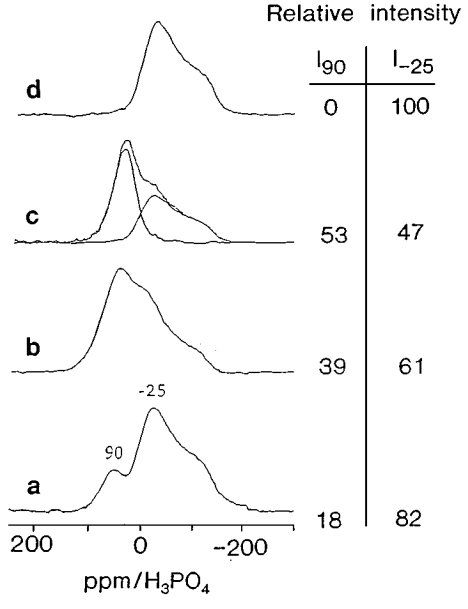

FIG. 4. ^{31}P NMR spin-echo mapping spectra: signals in the region (−200, +200 ppm) of PYRO-OX-1 (a), PYRO-OX-3 (b), PYRO-OX-24 (c), and PYRO-OX-24 after hot water leaching (d). The relative intensity of the two signals at 90 and −25 ppm has been indicated on the figure.

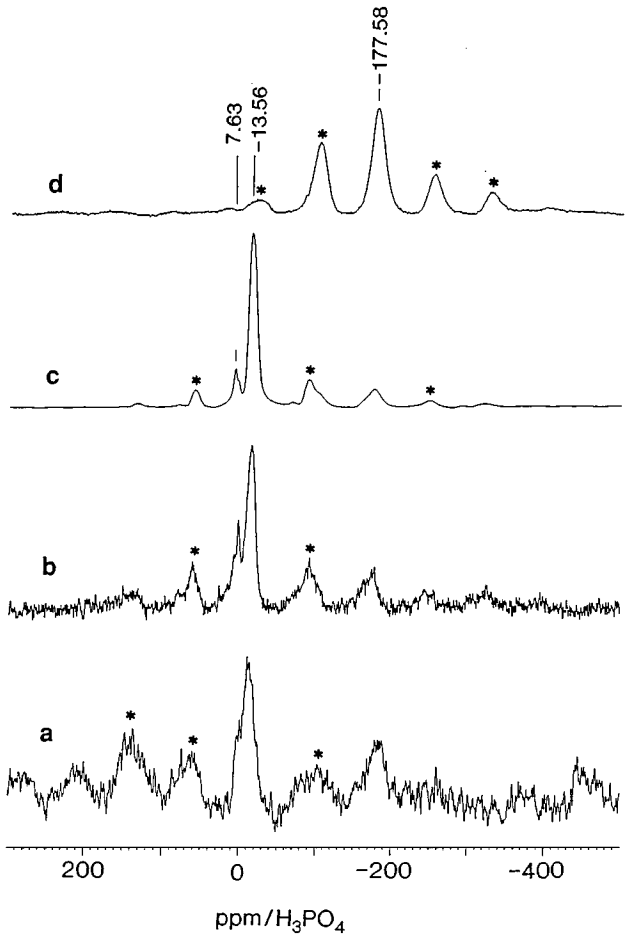

FIG. 5. ^{31}P NMR MAS of PYRO-OX-1 (a), PYRO-OX-3 (b), PYRO-OX-24 (c), and PYRO-OX-24 after hot leaching (d).

to these authors such defects are probably V^{5+} centers isolated and randomly distributed within some depth in the bulk of $(VO)_2P_2O_7$. Under such assumption, these bulk defects cannot be much affected by a water treatment, which explains why the corresponding signal is still present after washing PYRO-OX-24 with hot water (Fig. 5d).

Therefore, static as well as MAS NMR experiments tend to show that two kinds of V^{5+} species are formed upon oxidation of the pyrophosphate catalyst at 500°C. One of these species is characteristic of V^{5+} microdomains growing with oxidation time, probably located at the outer surface of the $(VO)_2P_2O_7$ crystals and dissolved readily in hot water. The other V^{5+} species are assigned to isolated centers associated with the creation of structural defects and randomly located throughout the crystals, at least within some depth.

DISCUSSION AND CONCLUSIONS

The aim of the present work was to better characterize the changes induced in a pure and well-crystallized $(VO)_2P_2O_7$ catalyst by treatments under an oxygen flow at 500°C. Note

that such treatments are very efficient with respect to the catalytic performance in the *n*-butane oxidation: the selectivity for MA increases from 52 to 84% (1) after 1 h of oxidation at 500°C. For longer times of oxidation, the selectivity slowly decreases. Besides the anisotropic creation of structural defects, XRD did not show the formation of any definite $VOPO_4$ phase. In agreement with DTA-TGA analysis and UV-VIS, XRD showed that the oxidation process is restricted to the surface region (1). This conclusion has been further ascertained by the techniques used in the present work: electrical conductivity, XPS, Raman, and ^{31}P NMR spectroscopic techniques.

Electrical conductivity measurements are quite informative on the enhanced catalytic performance of the oxidized catalysts which remain *p*-type semiconductors (6) but with an increased conductivity by creation of more anionic oxygen and positive holes p^+:

$$1/2\,O_2\ (g) \leftrightarrow O^{2-} + 2p^+.$$

As shown in Fig. 1, the redox cycle on the *in-situ* oxidized sample is rapid and quite reversible, supporting the creation of a pool of reactive surface O^{2-} species associated with the appearance of V^{5+} ions. It has to be recalled that surface lattice oxygen O^{2-} is directly involved in the formation of MA, as previously evidenced by ^{18}O labelling experiments (5). In a recent work we have shown by TPD (18) that O^{2-} species created by oxidation of $(VO)_2P_2O_7$ at 500°C are more labile and therefore more reactive. It is also important to stress the fact that, under the reaction mixture (Fig. 1), the sample remains much more oxidized than the starting $(VO)_2P_2O_7$ catalyst. This means that consumed surface O^{2-} (by reaction with *n*-butane) are replaced much more easily and more rapidly, with therefore a higher steady-state level of oxidizing power for the formation of oxygenates.

The present results further stress the importance of a suitable V^{5+}/V^{4+} balance (14, 19, 20). On the basis of the present XPS measurements, the best V^{5+}/V^{4+} surface ratio would be around 0.25 (one V^{5+} site for four V^{4+} sites). The nature of surface V^{5+} species, isolated or in microdomains, appears to be even more crucial than their amount. After oxidation of $(VO)_2P_2O_7$ at 460–500°C, Koyano *et al.* (21) reported the anisotropic oxidation of the (100) planes into the X_1 phase, most likely the same as δ-$VOPO_4$. The formation of δ-$VOPO_4$ was also claimed by Schuurman *et al.* (22) when a V-P-O catalyst was oxidized at 380–430°C. Although it must be admitted that the nature of the $VOPO_4$ phase must strongly depend on the experimental conditions of oxidation (temperature), the present study rather suggests the formation of α_I-$VOPO_4$ on the basis of laser Raman spectroscopy (band at 1038 cm^{-1}). However, the oxide formed at 500°C is not hydratable and remains a *p*-type semiconductor in contrast to the α_I-$VOPO_4$ phase (10). Furthermore, the present ^{31}P NMR results did not support the presence of α_I-$VOPO_4$. This prompted us to look for an alternative assignment of the Raman band at 1038 cm^{-1}. On the V_2O_5/TiO_2 Eurocat catalyst (23), a Raman band at 1033 cm^{-1} has been attributed to the V=O stretching vibration of isolated surface V^{5+}. In V_2O_5/Al_2O_3, catalysts active in *n*-butane partial oxidation (24), a Raman band at 1028 cm^{-1} has been evidenced in fully oxidized catalysts. This band was also assigned to isolated vanadyl species. Therefore we propose that the Raman band at 1038 cm^{-1} could be related to isolated V^{5+}=O on the $(VO)_2P_2O_7$ matrix. We have already proposed that such surface species could be formed upon mild oxidation of $(VO)_2P_2O_7$ as studied by TPD (18). The simultaneous presence of V^{IV} and V^{V} in the $(VO)_2P_2O_7$ lattice (mixed-valence state) has been recently investigated by Robert *et al.* (25) using quantum-chemical calculations. ^{31}P NMR analysis, both in the spin echo mapping and in the MAS mode, revealed that oxidation induced the development of two signals which could not be attributed to any definite $VOPO_4$ phase. These signals have been assigned to isolated V^{5+} species and to amorphous V^{5+} microdomains. These microdomains can be removed by hot water leaching, most likely because they have already some similar properties with $VOPO_4$ phases. Furthermore, they are expected to be located on the surface of the $(VO)_2P_2O_7$ matrix in the (100) face.

Conversely, V^{5+} species could be found within the bulk, likely with a gradient of concentration from the surface. One can imagine that oxidation proceeds first from nuclei, most likely crystal defects, steps, or kinks, on the $(VO)_2P_2O_7$ (100) faces which are preferentially exposed. Later on, these nuclei could yield clefts favoring the extension of the oxidation towards the bulk along the [100] axis. Such a mechanism of anisotropic oxidation could explain the creation of structural defects, associated with the presence of V^{5+} species in the $(VO)_2P_2O_7$ lattice, as previously suggested by the XRD spectra (1).

The selectivity for MA formation strongly increases at the early stage of oxidation, in parallel with the development of isolated V^{5+} sites in strong interaction with $(VO)_2P_2O_7$. These sites should be crucial in the selective oxidation of *n*-butane to maleic anhydride. Therefore controlled oxidation can be useful to activate the vanadyl pyrophosphate catalysts. The aim of such treatments is to achieve structural situations which provide suitable oxidizing power (redox state) required for the partial oxidation of *n*-butane. Such treatments are actually performed in the industrial Du Pont process (26) using a circulating fluidized bed reactor where the catalyst is reoxidized in a regenerator zone.

REFERENCES

1. Aït-Lachgar, K., Abon, M., and Volta, J. C., *J. Catal.* **171**, 383 (1997).
2. Bordes, E., *Catal. Today* **16**, 27 (1993).
3. Guliants, V. V., Benziger, J. B., Sundaresan, S., Wachs, I. E., Jehng, J. M., and Roberts, J. E., *Catal. Today* **28**, 275 (1996).
4. Bordes, E., and Contractor, R. M., *Topics Catal.* **3**, 365 (1996).

5. Abon, M., Béré, K. E., and Delichère, P., *Catal. Today* **33**, 15 (1997).
6. Herrmann, J. M., Vernoux, P., Béré, K. E., and Abon, M., *J. Catal.* **167**, 106 (1977).
7. Coulston, G. W., Bare, S. R., Kung, H., Birkeland, K., Bethke, G. K., Harlow, R., Herron, N., and Lee, P. L., *Science* **275**, 191 (1997).
8. Rodemerck, U., Kubias, B., Zanthoff, H. W., and Baerns, M., *Appl. Catal. A* **153**, 203 (1997).
9. Herrmann, J. M., *in* "Catalyst Characterization, Physical Techniques for Solid Materials" (B. Imelik and J. C. Védrine, Eds.), p. 559. Plenum, New York, 1994.
10. Rouvet, F., Herrmann, J. M., and Volta, J. C., *J. Chem. Soc. Faraday Trans.* **90**, 1441 (1994).
11. Ben Abdelouahab, F., Olier, R., Guillaume, N., Lefebvre, F., and Volta, J. C., *J. Catal.* **134**, 151 (1992).
12. Ben Abdelouahab, F., Volta, J. C., and Olier, R., *J. Catal.* **148**, 334 (1994).
13. Sananes, M. T., Tuel, A., and Volta, J. C., *J. Catal.* **145**, 251 (1994).
14. Abon, M., Béré, K. E., Tuel, A., and Delichere, P., *J. Catal.* **156**, 28 (1995).
15. Albonetti, S., Cavani, F., Trifiró, F., Venturoli, P., Calestani, G., Lopez-Granados, M., and Fierro, J. L. G., *J. Catal.* **160**, 52 (1996).
16. Delichere, P., Béré, K. E., and Abon, M., *Appl. Catal. A*, in press.
17. Nguyen, P. T., Sleight, A. W., Roberts, N., and Warren, W. W., *J. Solid State Chem.* **122**, 259 (1996).
18. Joly, J. P., Mehier, C., Bere, K. E., and Abon, M., *Appl. Catal. A* **169**, 55 (1998).
19. Cavani, G., Centi, G., Trifirò, F., and Grasselli, R. K., *Catal. Today* **3**, 185 (1988).
20. Sananes-Schulz, M. T., Tuel, A., Hutchings, G. J., and Volta, J. C., *J. Catal.* **166**, 388 (1997).
21. Koyano, G., Yamaguchi, F., Okuhara, T., and Misono, M., *Catal. Lett.* **41**, 149 (1996).
22. Schuurman, Y., Gleaves, J. T., Ebner, J. R., and Mummey, M. J., *in* "New Developments in Selective Oxidation II" (V. Cortés Corberán and S. Vic Bellón, Eds.), p. 203. Elsevier, Amsterdam, 1994.
23. Busca, G., and Zecchina, A., *Catal. Today* **20**, 61 (1994).
24. Wachs, I. E., Jehng, J. M., Deo, G., Weckhuysen, B. M., Guliants, V. V., and Benziger, J. B., *Catal. Today* **32**, 47 (1996).
25. Robert, V., Borshch, S. A., and Bigot, B., *J. Mol. Catal. A* **119**, 327 (1997).
26. Contractor, R. M., Garnett, D. I., Horowitz, H. S., Bergna, H. E., Patience, G. S., Schwartz, J. T., and Sisler, G. M., *in* "New Developments in Selective Oxidation II" (V. Cortés Corberán and S. Bellón, Eds.), p. 233. Elsevier, Amsterdam, 1994.